Journal Name

ARTICLE

One step microwave-assited synthesis of nanocrystalline WO_x-ZrO_2 acid catalysts

zReceived 00th January 20xx,
Accepted 00th January 20xx

DOI: 10.1039/x0xx00000x

www.rsc.org/

Francisco Gonell[a,b], David Portehault[c], Beatriz Julián-López[a], Karine Vallé[d], Clément Sanchez[c,*], Avelino Corma[a,*]

Nanocrystalline ZrO2 and WOx-ZrO2 catalysts with a good control over the zirconia phase and the nature of the W species were synthesized in a microwave-assisted aqueous route. The zirconia polymorphs monoclinic ZrO_2 (*m*-ZrO_2) and tetragonal ZrO2 (*t*-ZrO2) were isolated through an accurate control of the synthetic conditions, in acidic and basic media, respectively.

The evolution of the zirconia and W species under annealing of the WOx-ZrO2 nanocomposites at 500°C and 800°C was studied, and the resulting materials were tested as catalysts for the reactions of aldoxime dehydration and hydration of alkynes for the production of nitriles and carbonyls, respectively. In the dehydration reaction the most active species are W(VI) in tetrahedral coordination, independently of the ZrO_2 polymorph, while in the hydration reaction the zirconia phase plays a key role, as the tungsten doped t-ZrO2 appears the most active catalyst.

1. Introduction

A large number of acid-catalyzed industrial processes require the substitution of the aggressive and ecologically harmful mineral acids by solid acid catalysts that are stable, regenerable and active at moderate temperatures. Zirconia-based catalysts are promising candidates due to their thermal stability, structural versatility and surface properties.

The acid-base properties of zirconia depend on the crystalline phase, as ZrO_2 exhibits different polymorphs.[1] The thermodynamically most stable phase at room temperature and pressure is the monoclinic one, but depending on the synthetic methodology or by doping the material with different cations (Ce^{4+},[2] Ca^{2+},[3,4] La^{3+},[5] Y^{3+},[6] …), other metastable phases, like tetragonal and cubic ones, can be stabilized and isolated as single phases.

The acid properties of zirconia can be adjusted by the addition of sulfate,[7] Mo(VI)[8] or W(VI)[9] ions. Among these modified zirconia, tungsten-deposited zirconia is the most interesting candidate because the sulfated zirconia undergoes partial deactivation due to sulfate loss during thermal treatment,[10] while the molybdenum-doped zirconia is a less active catalyst. Since the first work of Hino and Arata[11,12] demonstrating the use of tungsten-deposited zirconia as a solid acid for isomerization of light alkanes, several reactions such as oxidative desulfurization,[13] alkylation of phenols,[14] o-xylene isomerization,[15] production of aromatics from alkylfurans,[16] 2-butanol dehydration,[17] among others, have been catalyzed by these materials. Herein, we focus on the industrially relevant aldoxime dehydratation and alkyne hydration reactions, for the synthesis of nitriles and carbonyl compounds, respectively.

On one side, nitriles are a family of organic compounds used as intermediates for the production of pharmaceuticals, agricultural chemicals dyes and materials.[18,19] Among the several synthetic pathways reported to obtain nitriles,[19] catalytic dehydration of aldoximes is the most efficient. This reaction has been classically catalyzed by homogeneous catalysts,[20,21,22] including H_2SO_4.[23,24] However the use of a heterogeneous catalyst may be a step forward towards an eco-friendly process. In this sense, some heterogeneous catalysts have been reported,[25] but they usually involve precious (Ru)[26] or toxic (Sn)[27] elements.

On the other side, alkyne hydration discovered in 1860[28] has become an industrially important reaction producing carbonyl

[a] Departament de Química Inorgànica i Orgànica and Institute of Advanced Materials (INAM), Universitat Jaume I, Av. Vicente Sos Baynat, s/n, 12071 Castelló, Spain.
[b] Instituto Universitario de Tecnología Química CSIC-UPV, Universitat Politècnica de València, Av. De los Naranjos, s/n, 46022 Valencia, Spain. E-mail: acorma@itq.upv.es
[c] Sorbonne Universités, UPMC Univ Paris 06, CNRS, Collège de France, Laboratoire de Chimie de la Matière Condensée de Paris, 11 place Marcelin Berthelot, 75005 Paris, Frane. E-mail: clement.sanchez@college-de-france.fr
[d] CEA DAM Le Ripault F-37260, Monts, France.

Electronic Supplementary Information (ESI) available: Experimental section (synthesis protocols and characterization techniques). Characterization of the materials and catalytic results not shown in the manuscript. See DOI: 10.1039/x0xx00000x

compounds. Traditionally, this reaction is carried out in the presence of Brønsted or Lewis acids as catalysts. Among them, Hg[29,30] salts are the most efficient but they are highly toxic. Other metals such as Au[31], Ru[32] or Fe[33] also present high efficiency, but recycling their salts is tedious. In the last years, some reports on the use of alternative heterogeneous catalysts for alkyne hydration have been presented, but their usefulness is limited due to the necessity of using homogeneous cocatalysts,[34,35] expensive precious metals (Au[35] or Ag[36]) or toxic elements (Sn[37]). We show in this report that W-modified zirconia nanoparticles are promising heterogeneous catalysts for aldoxime dehydratation and alkyne hydration.

Several synthetic pathways have been proposed to synthetize W/ZrO_2 materials, such as deposition of tungsten salts over hydrous zirconia,[11,38] anion exchange,[39,40] coprecipitation,[41,42] hydrothermal synthesis,[43] or the sol-gel process.[44] In the three latter methods mentioned, treatments at relatively high temperatures are required in order to activate the materials, probably because the tungsten ions are located inside the zirconia and have to migrate to the surface in order to be catalytically active. Moreover, several authors have pointed out that impregnating tungsten salts over already crystalline zirconia yields much less active catalysts than the impregnation of a disordered hydrous oxo-zirconium support.[12,45] Beyond the aforementioned preparation methods, other colloidal synthesis approaches based on microwave irradiation are developed since few years.

Microwave-assisted synthesis of solid materials presents several advantages over the synthetic pathways cited above, because it relies on heating directly the whole reaction volume, rather than by heat diffusion across the reaction vessel. This feature results in short reaction times (just few minutes to obtain crystalline materials), homogenous temperature inside the synthesis medium, thus avoiding temperature gradients and heterogeneities, and the possibility to control particle morphology and size by an accurate tuning of the synthetic conditions. Thus, microwave-assisted methodologies offer new opportunities to develop low cost and easy-to-prepare heterogeneous catalysts such as W-doped ZrO_2 that can be of interest for different reactions. To our knowledge, such synthetic methods have not been reported so far for tungsten-modified zirconia nanocrystals.

In this paper we propose a one-step, fast and environmentally friendly microwave-assisted synthesis of WO_x-ZrO_2 in which the zirconia crystal phase and the distribution of W species can be tuned through an accurate control of the synthetic conditions. These materials have an important impact as catalyst for the aldoxime dehydration and alkyne hydration. The catalytic activity and reaction mechanisms are discussed with respect to the zirconia crystal phase and the nature of the W species present in the final materials.

2. Results and Discussion

2.1 Microwave-assisted synthesis of ZrO_2-based naterials

Briefly, the materials were synthesized from an aqueous solution of zirconium oxychloride and the appropriate amount of sodium tungstate (Scheme 1). In so-called “acid route” (“ZA” samples), this solution was heated in a dedicated microwave-oven at 220°C

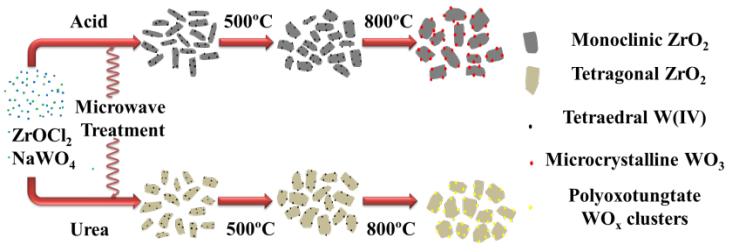

Scheme 1. Microwave-assisted WO_x-ZrO_2 synthesis. ZrO_2 phase and W species tuning upon acid or urea synthesis.

for 10 min. In the “urea” route (“ZU” samples), some urea was added to the initial solution to yield a pH increase upon its decomposition. The evolution of the crystalline phase in the WO_x-ZrO_2 system with respect to synthesis conditions (acid/basic media) and the W content has been studied first (Scheme 1). Powder X-ray diffractograms (PXRD) shows that the non-doped ZA zirconia exhibits solely the monoclinic phase, while the non-doped ZU zirconia is mostly made of the tetragonal phase (89 vol. % evaluated from the relative intensities of specific XR reflections, see Supporting Information (SI)).

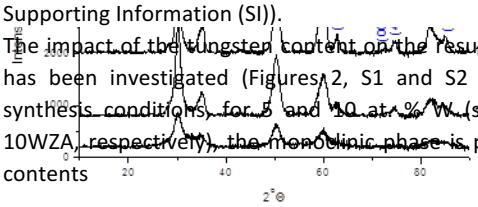

The impact of the tungsten content on the resulting zirconia phase has been investigated (Figures 2, S1 and S2 in SI). In the acid synthesis conditions, for 5 and 10 at. % W (samples 5WZA and 10WZA, respectively), the monoclinic phase is preserved for all W contents (

Figure **2**a and Figure S1b). On the contrary, upon addition of 5 to 10 at. % of tungsten in the urea synthesis (samples 5WZU and 10WZU, respectively), the tetragonal phase is stabilized, with a corresponding volume fraction of 89, 95 and 100 vol. % for ZU, 5WZU and 10WZU, respectively (Figure 2b and Figure S2b). The molar tungsten and zirconium percentages measured by inductively coupled plasma atomic emission spectroscopy (ICP-AES) (Table S1) are close to the initial ratios of precursors, thus showing that all tungsten and zirconium species precipitate.

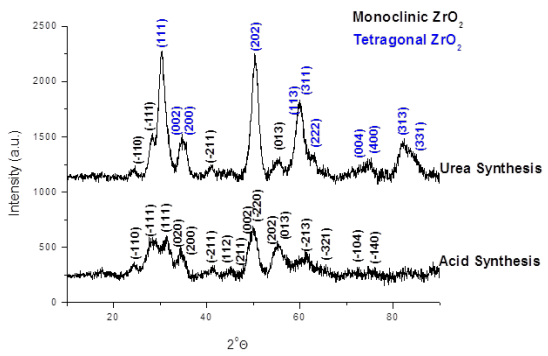

Figure 1. XRD patterns of as-synthesized un-doped zirconia powders prepared by the urea- (ZU) and acid-based (ZA) syntheses.

The thermal stability of these materials was studied by thermogravimetric analysis under air (Figure S3). In the 10WZA sample, a mass loss of around 7 wt. % at 250°C is associated to the removal of water molecules adsorbed at the surface. Another mass loss of around 3 wt. % occurs at 450°C, which is probably due to the loss of structural hydroxyl species. The 10WZU sample shows larger weight losses, around 10 wt. % for the first process, and 5 wt.% loss in a two steps, which correspond to the same processes commented for 10WZA. FT-IR of the as prepared samples and calcined at 500 and 800°C were perfomed. In this experiment a decrease of band intensity corresponding to OH upon heating was observed (Figure S4) confirming the primary.

The phase evolution with the annealing temperature was studied by XRD (Figure 2 and Figures S1 and S2). For the acid procedure, the tungsten-free (ZA) and the 5 at. % W-doped (5WZA) samples (Figure S1) present at all calcination temperatures the monoclinic phase as only crystalline phase, with sharper and narrower peaks as the temperature increases. No peaks associated to WO_3 species are observed, suggesting that tungsten is highly dispersed and/or incorporated into the ZrO_2 matrix. For the 10WZA sample (Figure 2 a), the monoclinic phase is again the only crystalline phase (100%) until 500°C, but at 800°C reflections associated to crystalline monoclinic WO_3 and tetragonal ZrO_2 phase (around 13 vol.%) appears together with the *m*-ZrO_2 peaks.

The percentage of the tetragonal phase, the zirconia crystal size calculated from XRD by the Scherrer equation and the BET surface

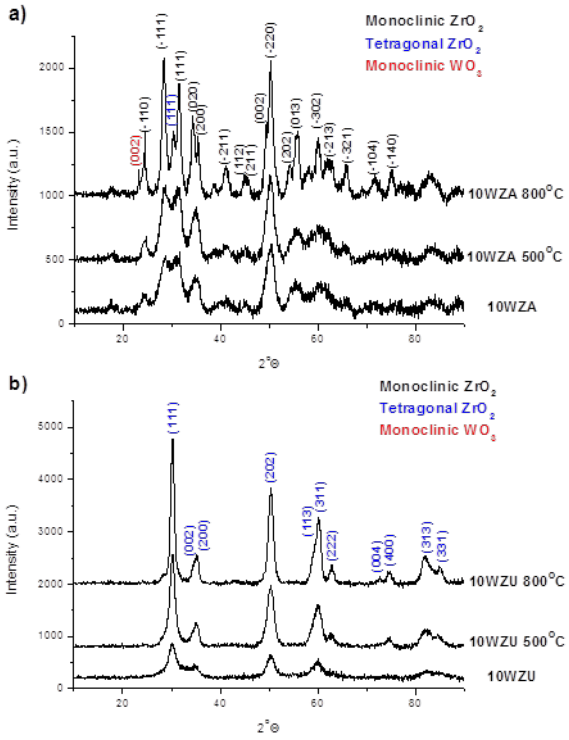

Figure 2. XRD patterns of a) 10WZA and b) 10WZU powders as prepared and annealed at 500°C and 800°C.

Table 1. Volume percentage of the tetragonal phase, zirconia crystal size calculated by the Scherrer equation and BET surface areas of the materials obtained by the synthesis in acidic medium.

Sample	Vol. % Tetragonal	Crystal Size (nm)	S_{BET} (m^2/g)
ZA	0	2	210
ZA 500°C	0	8	65
ZA 800°C	0	17	22
5WZA	0	3	213
5WZA 500°C	0	5	109
5WZA 800°C	0	10	51
10WZA	0	3	222
10WZA 500°C	0	4	137
10WZA 800°C	13	10	57

area of the materials prepared under acidic conditions are compiled in Table 1. The non-annealed materials present similar BET surface area values of ca. 220 m^2/g. Upon annealing, small crystal sizes and large areas are best preserved for higher W contents. This trend can be explained by the presence of WO_x surface species, which inhibit the surface mobility of Zr and O species on zirconia, thus limiting the sintering process and keeping high surface area values.[9] Another explanation might arise from the stabilizing effect of W species which substitute hydroxyl groups and defects at the surface.[39]

The thermal evolution of the materials synthesized under basic conditions is different. The as-synthesized non-doped sample (ZU) mostly occurs in a tetragonal phase (89 vol. %). However upon

annealing, the monoclinic phase becomes the major zirconia polymorph, with only 36 vol. % of the tetragonal phase remaining at 500°C, while the material is completely monoclinic under the form at 800°C (Figure S2a and

Table 2). A significant stabilization of the tetragonal phase is observed in the materials after doping with W species, with 100, 96 and 85 vol. % of tetragonal polymorph in 5WZU for the as-synthesized sample and those annealed at 500°C and 800°C, respectively (Figure S2b and

Table 2). The material doped with 10% W molar (10WZU) presents pure tetragonal phase at all temperatures (Figure 2 b and

Table 2). 10WZU was further

Table 2. Volume percentage of the tetragonal phase, zirconia crystal size calculated by the Scherrer equation and BET surface areas of the materials obtained by the urea-based synthesis.

Sample	Vol. % Tetragonal	Crystal Size (nm)	S_{BET} (m^2/g)
ZU	88	5	137
ZU 500°C	36	8	53
ZU 800°C	0	23	78
5WZU	100	5	172
5WZU 500°C	96	9	107
5WZU 800°C	84	12	44
10WZU	100	4	298
10WZU 500°C	100	6	140
10WZU 800°C	100	10	67

annealed at 900°C, thus leading to crystallization of monoclinic WO_3, together with the sole monoclinic zirconia (Figure S5). Moreover, as in the synthesis in acidic conditions, the addition of W in the sample limits sintering and loss of BET surface area **(**

Table 2). The W atomic percentage is preserved in all the materials after the different thermal treatments as measured by ICP-AES (Table S1), thus pointing out that no W is lost during the calcination steps.

XRD provides information about the crystalline phase of zirconia but is not suitable to address the nature of the poorly crystalline tungsten species. Thus, the samples were characterized by Raman spectroscopy that is a powerful tool to elucidate the nature of W species.[9 15]

The Raman spectra of tungsten-free ZA and ZU samples calcined at different temperatures are given in the Supporting Information (Figure S6). The spectra of ZA show the typical bands corresponding to monoclinic ZrO_2 (637 (s), 618 (s), 558, 537 (w), 504, 477 (s), 381, 343, 335, 305, 221 (w), 187 (s) and 177cm^{-1})[46] at all temperatures.

The spectra of ZU exhibit the typical bands of both monoclinic and tetragonal ZrO_2 (639 (s), 604 (sh), 462 (s), 313 (s), 271 (s) and 149 (s) cm^{-1}),[46] but the tetragonal phase disappears upon temperature increase, in good agreement with XRD. In the W-doped samples, the Raman zirconia bands follow also the same tendency observed

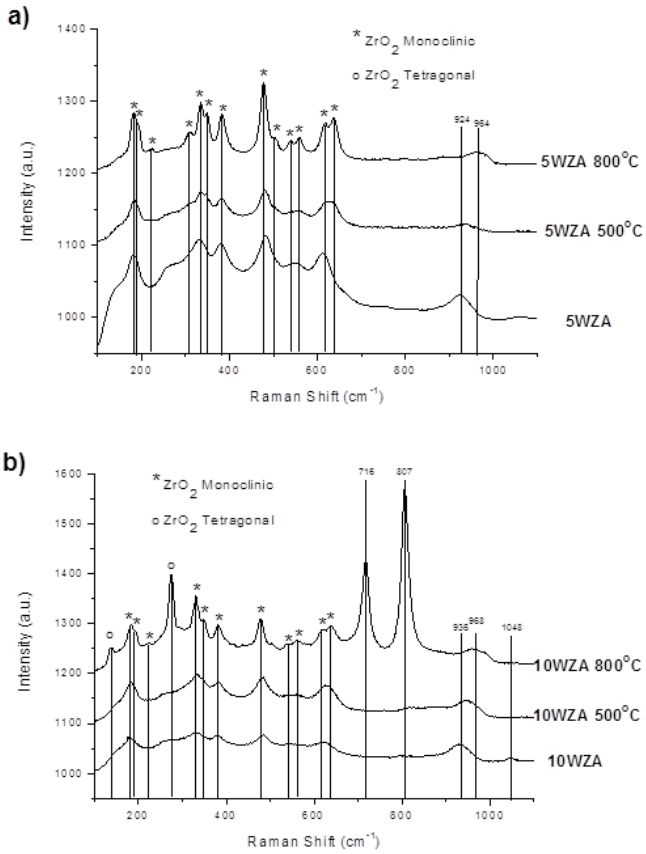

Figure 3. Raman spectra of a) 5WZA and b) 10WZA samples as-prepared and annealed at 500°C and 800°C.

in XRD. Interestingly, in the range where the bands associated to W species usually appear (from 700 to 1100 cm^{-1}), significant differences are found (**¡Error! No se encuentra el origen de la referencia.**).

W-doped ZA samples show a band around 930 cm^{-1} attributed to the A_1 mode (ν_1 symmetric stretching vibration) of tetrahedral W(VI) cations,[39 43] which shifts towards larger wavenumbers (945 cm^{-1}) when the material is annealed at 500°C, probably due to the condensation of the tungsten species.[43] At 800°C, different bands depending on the W content are detected. Both 5WZA and 10WZA samples present a band around 965 cm^{-1} corresponding to the W=O stretching mode, while 10WZA exhibits also two intense bands at 716 and 807 cm^{-1} associated to W-O-W and W=O stretching modes of microcrystalline monoclinic WO_3 species.[13,16]

In basic conditions (Figure 4), the as-prepared 5WZU and 10WZU materials show the previous W-related band at 940 cm^{-1} and a new one at 840 cm^{-1}, which correspond to the A_1 and F_2 (ν_3

antisymmetric stretching vibration) modes of tetrahedral W(VI) cations, respectively. In these samples, we also find at 1050 cm^{-1} a band attributed to carbonates neutralizing the basic sites unoccupied by tungstates for low W contents.[39] At 500°C, this band at 1050 cm^{-1} disappears while the others remain almost constant, showing that carbonates are eliminated from the zirconia surface.

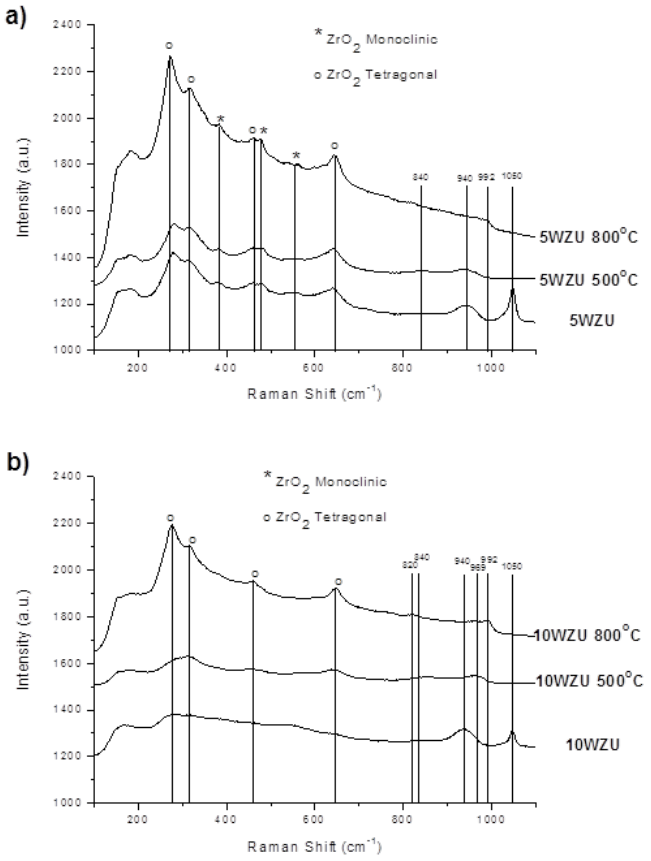

Figure 4. Raman spectra of a) 5WZU and b) 10WZU powders as prepared and calcined at 500°C and 800°C.

At 800°C, two bands located at 820 and 992 cm^{-1} assigned to W-O-W and W=O stretching modes of hydrated interconnecting polyoxotungstate clusters are visible[9 13 39]: From the Raman data, one can conclude that after annealing at high temperature, tungsten is better dispersed starting from the tetragonal phase (WZU samples) rather than the monoclinic one (WZA samples), since features of molecule-size clusters are still observed in the WZU samples. This behavior is quite different from Mo species supported on different zirconia polymorphs in which a better dispersion of Mo species is obtained on the monoclinic phase, mainly due to the presence of 2D polymolybdate species. Meanwhile in the tetragonal phase, crystalline MoO_3 is observed. This behaviour also affects the catalytic activity, as a lower Mo dispersity is detrimental to the catalytic rates in methanol oxidation.[46]

The morphology of the different samples was studied by transmission electron microscopy (TEM). Under acid conditions, the pure zirconia ZA sample (Figure 5 a) is obtained as rod-like nanocrystals (10 x 3 nm) agglomerated into 40 nm diameter urchin-like particles, while well dispersed 5 nm nanoparticles are found in the pure ZU sample (Figure 5 b). The addition of W in the system induces slight morphological changes. In acid conditions, small "quasi-spherical" particles of 4 nm instead of rods are detected (Figure 6a); these particles agglomerate into slightly denser aggregates than in the case of non-doped samples. Under basic conditions, no significant morphological changes occurred upon

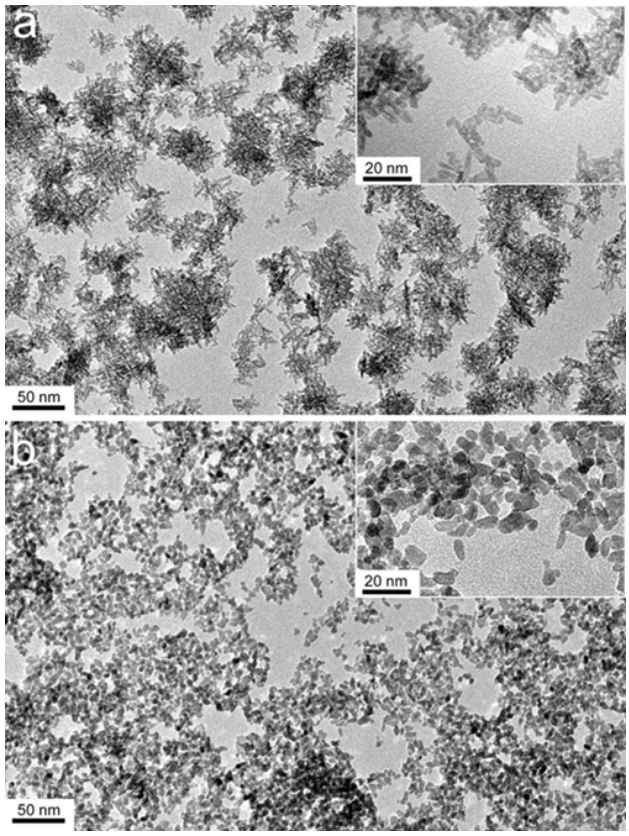

Figure 5. TEM micrographs of a) ZA and b) ZU samples as prepared.

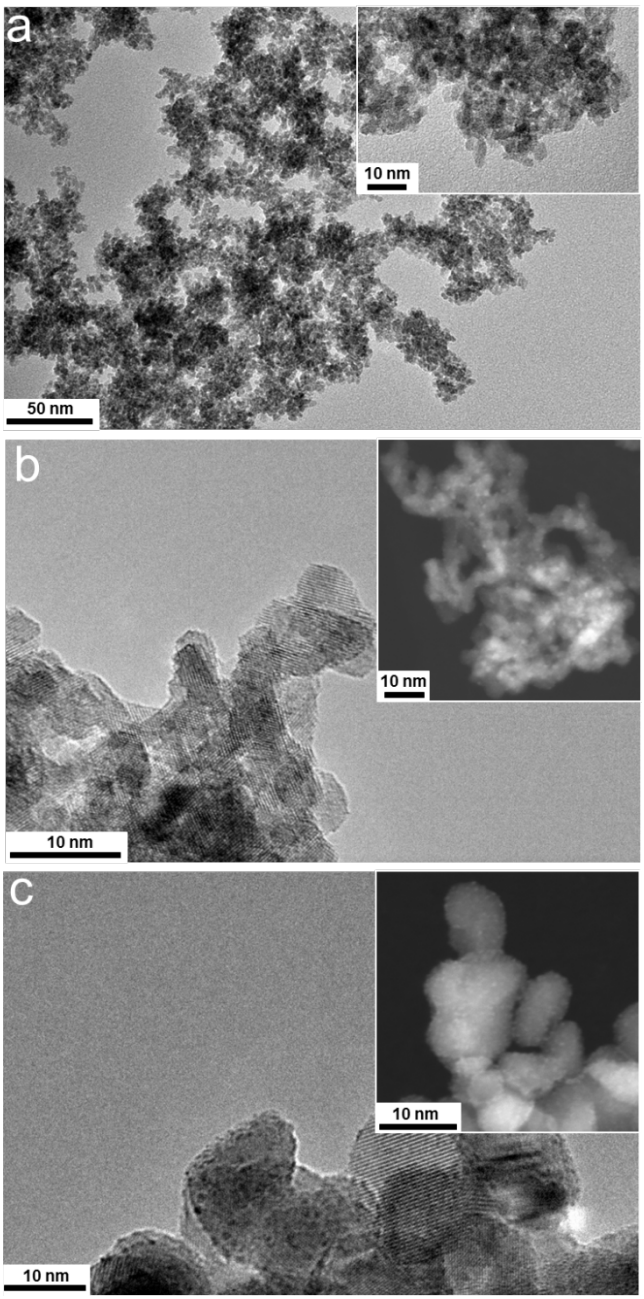

Figure 6. a) TEM micrographs of 10WZA as prepared, b) HRTEM and HAADF-STEM micrographs (insets) of 10WZA annealed at 500°C and c) at 800°C

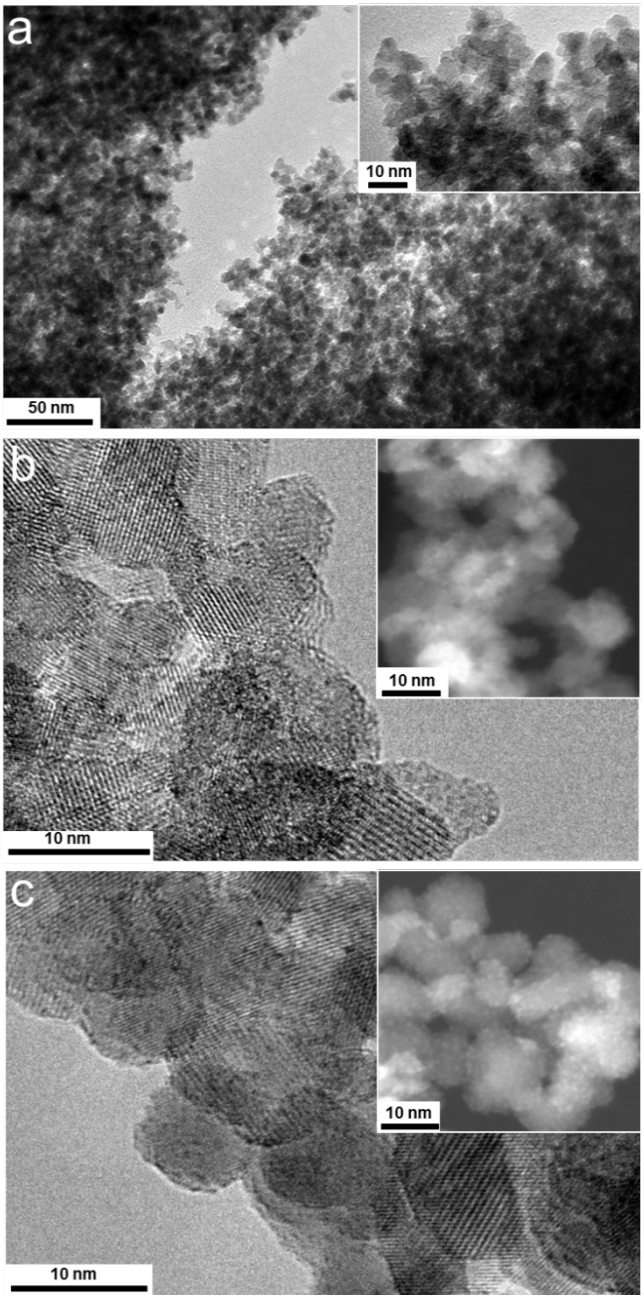

Figure 7. a) TEM micrographs of 10WZU as prepared, b) HRTEM and HAADF-STEM micrographs (insets) of 10WZU annealed at 500°C and c) at 800°C

addition of tungsten (Figure 7a). With the thermal treatment, surface tungsten species become visible in HRTEM in the form of dark spots in bright field and bright spots in HAADF-STEM, the latter providing contrast as a function the atomic number. Indeed, the 10WZA sample exhibits small spots at the surface of the 5 nm zirconia particles after annealing at 500°C (Figure 6 b). The phenomenon is more apparent after annealing at 800°C (Figure 6 c). These spots of less than 1 nm are interpreted as the crystalline monoclinic WO_3[47] phase detected by XRD and Raman spectroscopy for 10WZA annealed at 800°C.

In the 10WZU sample calcined at 500°C (Figure 7b), small spots are also visible. According to Raman data, they are attributed to W(VI) species in tetrahedral coordination. At 800°C, the images show very small nanoparticles (few angstroms) that could be associated to polyoxotungstate clusters,[41 48 49] in agreement with Raman spectroscopy.

The dispersion and oxidation state of W of the different samples were determined by X-ray photoelectron spectroscopy (XPS). The

signal of W_{4f} was fitted using two components which correspond to W^{6+} (ca. 35.6 eV) and W^{5+} (ca. 34.5 eV) (Figure S7). The ratio W^{6+}/W^{5+} increase upon increasing the calcination temperature (see Table S2), this fact is caused because in the as prepared materials the high dispersion of tungsten atoms in zirconia induce a strong interaction between zirconium and tungsten which induce high content of tungsten in the lower oxidation state. Upon heating, the different tungsten species are formed, decreasing the interaction with zirconia an increasing the content fo W^{6+}. The ratio W/Zr follows the same trend for 10WZA and 10WZU upon heating. In the as prepared sample the high dispersion of tungsten atoms in zirconia and the small size of the particles lead to high W/Zr ratio. Upon heating at 500°C this ratio decreases because of the formation of tungsten patches in tetrahedral coordination, doing zirconium more visible. Finally at 800°C the rartio decreases because the particles grow to 10 nm and part of the zirconium is not detected (depth analysis 6.5nm).

The acid type, strength and density were evaluated by adsorption and desorption of pyridine at different temperatures (Figure S8 and Table S3). For samples calcined at 500°C (10WZA500 and 10WZU500) only Lewis acid sites are observed with similar density and strength which may correspond to the acidity of tetrahedral W(VI). For samples calcined at 800°C (10WZA800 and 10WZU800) both samples present similar Lewis acid sites at lower desorption temperature but the strength of this sites in 10WZU are higher. Moreover much higher Brønsted acidity and strength are observed in 10WZU800 compared to 10WZA800. These acid differences may rely on the different tungsten species present in these materials discussed above.

Three different materials from the literature were also synthesized to provide references for the catalytic properties microwave-derived materials. They are a mixed Sn-W oxide (in a molar ratio 2Sn:1W, denoted SnW-2:1), zirconia doped with W at 10 mol. % prepared by coprecipitation (denoted 10WZDis), and another W-doped zirconia with the same W content but obtained from impregnation techniques (denoted 10WZDep) (see SI). These samples were also annealed at 500°C and 800°C.

The XRD pattern of SnW-2:1 (Figure S6a) shows the pure rutile structure (casiterite, SnO_2), thus demonstrating that tungsten is highly dispersed or incorporated into the SnO_2 matrix, in good agreement with Ogasawara et al.[50] Similarly to the microwave-derived samples, at 800°C, XRD peaks of microcrystalline WO_3 appear in the pattern (Figure S9). The as-prepared reference zirconia samples 10WZDep and 10WZDis are amorphous (Figure S9 b and c). After annealing, the main zirconia phase is the tetragonal one in both cases. Again, at 800°C, microcrystalline WO_3 is detected. Crystal sizes calculated by the Scherrer equation and BET surface area are compiled in Table S4. The values are similar to those obtained for the microwave-derived materials, which is of outmost importance for comparing the catalytic activities.

The results detailed above in microwave-assisted synthesis demonstrate that the zirconia crystalline phase can be tuned from monoclinic to tetragonal by changing the pH conditions (acid to basic, respectively). In addition, high tungsten doping levels induce a phase transformation towards the tetragonal phase. Annealing yields the thermodynamic phase, which is monoclinic zirconia. For the non-doped samples, the morphology can also be changed from rod-like to more spherical nanoparticles, and from aggregated to more dispersed systems by changing the pH of the synthesis medium from acid to basic conditions. For W-doped samples, different W species have been detected by TEM and identified by Raman spectroscopy. Their nature strongly depends on the thermal treatment and the synthesis conditions.

In comparison to 10WZA and 10WZU with the reported references materials 10WZDep and 10WZDis prepared by impregnation or coprecipitation respectively, the microwave-assisted synthetic approach allows obtaining as-prepared nanocrystalline materials of few nanometers with a controlled morphology. The crystal sizes measured by XRD are almost twice for the reference materials compared to those obtained by the microwave-derived route, independently of the tungsten content and the annealing temperature (Tables 1, 2 and S1). Consequently, the microwave route provides a highly dispersed catalyst. Furthermore, adjusting the pH in the microwave-assisted synthesis provides an efficient way to tune the nature of the catalytic W sites and possibly the catalytic activity.

2.2 Formation mechanism of *m*- and t-ZrO_2 under microwave synthesis

The formation mechanism of the nanoparticles was further studied carrying out the microwave synthesis in the same reaction conditions, but quenching the reaction medium at different temperatures and times. The XRD patterns of the different materials are compiled in Figure S12 and S13. The materials synthesized in acid conditions at 120°C are amorphous. After 1 min at 170°C, very weak peaks of the *m*-ZrO_2 are superimposed to the amorphous background. By increasing the reaction time and temperature (220°C for 1 min and 220°C for 10 min), the XRD peaks of the monoclinic polymorph become narrower, indicating an increase in the crystallinity. In the urea-based synthesis, the first diffraction peaks appear at higher reaction times and temperatures (170°C/10 min). At 220°C/1min, more defined diffraction peaks are observed whose intensity increases with temperature and time, thus leading mostly to *t*-ZrO_2, with *m*-ZrO_2 as a minor product.

The different materials were also characterized by Raman spectroscopy (Figure S14 and S15). The sample treated at low temperature in the acid route shows broad peaks at 151, 260, 405 and 546 cm^{-1}. The two first signals can be assigned to the tetragonal ZrO_2 polymorph[51] while the two others correspond to hydrolyzed polymeric zirconium species.[52–55] At higher temperatures, bands corresponding to *m*-ZrO_2 appear, becoming narrower as the temperature increases while the peak of *t*-ZrO_2 is still observed. This fact indicates that minor amounts of *t*-ZrO_2 coexist with *m*-ZrO_2, although it was not detected by XRD. For the samples obtained by the urea method, at low temperature the same bands are observed as for the acid method except the *t*-ZrO_2 signal around 260 cm^{-1}. Increasing the temperature and time yields the appearance of this *t*-ZrO_2 peak and other peaks characteristics of *m*-ZrO_2, in good agreement with the XRD analysis.

TEM (Figure S16 and S17) highlights the evolution of the morphology of ZrO_2 synthesized in acid and in urea aqueous media. For the acid synthesis, at 120°C an amorphous dendritic sol is observed which still remains at 170°C with denser aggregates

without any clear morphology. These aggregates could be assigned as incipient monoclinic nuclei, according to the XRD and Raman analysis. At this temperature, if the reaction time is prolonged, rod-like nanoparticles (10 x 3 nm) agglomerated into 40 nm particles appear, this morphology is preserved when the reaction temperature is increased to 220°C at different reaction times (Figure S13). On the other side, the materials obtained with the urea method remain amorphous until 170°C/10 min where we can observe some crystalline fringes immersed in the amorphous particles. Increasing the temperature to 220°C/1min increases the crystallinity of the sample while the nanoparticles boundaries begin to be clearly observed. Finally at 220°C/10min well defined crystalline nanoparticles are obtained.

When $ZrOCl_2{\cdot}8H_2O$ is dissolved in water, cyclic $[Zr(OH)_2{\cdot}4H_2O]_4^{8+}$ tetramers (which consist in four Zr^{4+} atoms forming a square linked by two OH groups, and four molecules of water filling out the coordination sphere of the zirconium atoms) are the major species in solution.[56 57] Starting from this soluble precursor, the acidic and urea synthesis routes lead preferably to *m*-ZrO_2 and *t*-ZrO_2, respectively. It is possible to explain this phase selection by considering differences in the solubility of Zr species in acidic and basic media. For the acid synthesis, upon heating, the tetramers polymerize via hydroxyl binding and olation,[58 59] forming an amorphous hydrous zirconia sol $[ZrO_x(OH)_{4-2x}{\cdot}yH_2O]_n$. Previous works have shown that the short range order of such amorphous phase is very close to the structure of tetragonal ZrO_2[60] (120°C/10min), in agreement with our Raman data (Figure S14). Upon increasing the temperature and time, the vast majority of Zr species crystallize into monoclinic zirconia (170°C/1min), the thermodynamic phase in the synthesis conditions. The transformation from the amorphous form with the local order of the tetragonal phase into the monoclinic form is enabled by a dissolution-recrystallization mechanism through the significant solubility of zirconium species in acidic media.[61 62] For the urea synthesis, upon heating, urea hydrolyzes to CO_2 and NH_3 at ca. 80°C, thus increasing the pH and leading again to the precipitation of amorphous hydrous zirconia. In such conditions, the solubility of Zr species is low.[61 62] Hence the amorphous phase crystallizes by *in situ* transformation that results in minimal ion displacements. Consequently, amorphous zirconia with the local order of the tetragonal phase evolves towards *t*-ZrO_2. The observed slight amounts of *m*-ZrO_2 originate from the non-negligible solubility that allows partial dissolution and recrystallization of the thermodynamic monoclinic phase.

2.2 Catalytic results

2.2.1 Synthesis of nitriles from aldoximes

The catalytic activity of all the materials was tested in two different reactions requiring acid catalysis, namely aldoxime dehydration (Scheme 2) and alkyne hydration (Scheme 3).

In the aldoxime dehydration, pure zirconia (ZU and ZA) show very poor catalytic activity, with a maximum conversion of ~38% for the as-synthesized ZA sample. The activity diminishes for the annealed catalysts down to 10% conversion (for ZU-800). In all cases, the materials synthesized by the acid route exhibits slightly higher activity (~ 5% conversion higher) than those synthesized by the basic route. In any case, the selectivity toward the cyano product is not higher than 60%, leading to benzamide or benzaldehyde as by-products (Scheme S1 and Table S5).

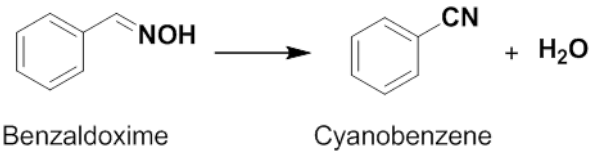

Scheme 2: Benzaldoxime dehydration reaction to cyanobenzene (Cyano).

Table 3 and Table 4 show the catalytic activity for aldoxime dehydration of the W-doped samples prepared in acid and basic conditions. For 5WZA (

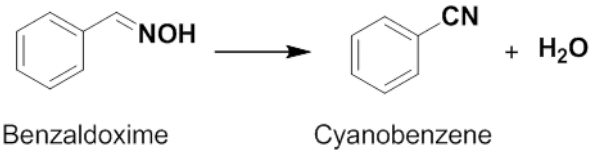

Scheme 2: Benzaldoxime dehydration reaction to cyanobenzene (Cyano).

Table 3), the conversion of the oxime is higher as the annealing temperature of the catalyst increases, but the highest selectivity is obtained for 5WZA-500 (90%). On the other hand, for 10WZA, the highest conversion and best selectivity towards the cyano product (98% and 92% respectively) are obtained for an annealing temperature of 500°C.

In the samples prepared under basic conditions (Table 4), the highest activity and selectivity is observed for the catalysts annealed at 500°C, independently of the W content. A general tendency in the samples WZA and WZU is that by increasing the amount of W conversion and the selectivity towards the desired product increase

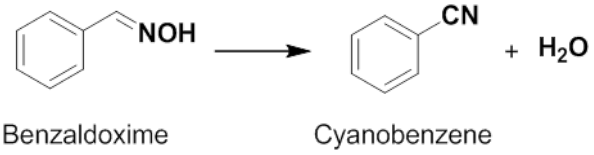

Scheme 2: Benzaldoxime dehydration reaction to cyanobenzene (Cyano).

Table 3. Conversion, yield, selectivity and initial rate towards aldoxime dehydration of X-WZA-Y. Reaction Conditions: Catalyst 50 mg, 0.50 mmol Benzaldoxime, nitrobenzene as standard, 1.5 mL o-xylene, 150°C, 5h.

Catalysts	X Oxime (%)	Y Cyano (%)	Sel. Cyano (%)	Initial rate/ S_{BET} (g/h·m^2)
5WZA	53.6	43.7	81.5	0.05
5WZA500	71.0	64.1	90.3	0.14
5WZA800	94.1	78.9	83.8	0.54
10WZA	85.4	76.5	89.6	0.10
10WZA500	**97.8**	**89.7**	**91.7**	**0.25**
10WZA800	85.0	72.6	85.3	0.39
10WZA500used	97.2	86.3	88.8	-

In the samples prepared under basic conditions (Table 4), the highest activity and selectivity is observed for the catalysts annealed at 500°C, independently of the W content. A general tendency in the samples WZA and WZU is that by increasing the amount of W conversion and the selectivity towards the desired product increase.

Notice that by using microwave-assisted synthesis, the best materials 10WZA500 and 10WZU500 reach conversions and selectivities of ca. 98% and 90%, respectively, while all reference catalysts show lower activity and selectivity (see Table S6).

According to these results, the large amount of hydroxyl groups at the surface of the as-prepared catalysts appears as detrimental for aldoxime dehydration. Once these hydroxyls are removed at 500°C, catalytic results improve, although further annealing at 800°C leads to a decrease in the activity and selectivity, because of a decrease in the dispersion and surface area. In addition, the higher the tungsten content (10 at. %W), the more active the catalyst is.

When normalizing the initial rate *versus* the BET surface area (

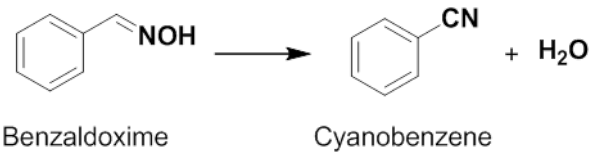

Scheme 2: Benzaldoxime dehydration reaction to cyanobenzene (Cyano).

Table 3 and Table 4) it can be seen that the specific activity of the materials increases as the annealing temperature increases, despite the fact that the materials calcined at 500°C are the most active and selective. This fact can be explained on basis of acidity that presents these materials, thus the Lewis acid sites and strength that present 10WZA500 and 10WZU500 seems to be the best for this reaction compared to the acidity that present 10WZA800 and 10WZU800.

Table 4. Conversion, yield, selectivity and initial rate towards aldoxime dehydration of X-WZU-Y. Reaction Conditions: Catalyst 50 mg, 0.50 mmol Benzaldoxime, nitrobenzene as standard, 1.5 mL o-xylene, 150°C, 5h

Catalysts	X Oxime (%)	Y Cyano (%)	Sel. Cyano (%)	Initial rate/ S_{BET} (g/h·m^2)
5WZU	62.8	49.8	79.2	0.08
5WZU500	80.8	69.9	86.5	0.14
5WZU800	49.4	39.1	79.1	0.20
10WZU	69.2	58.5	84.6	0.05
10WZU500	**98.2**	**87.6**	**89.3**	**0.25**
10WZU800	72.0	60.6	84.2	0.21
10WZU500used	97.9	87.2	89.1	-

Since the crystalline phase of the zirconia is very different in the materials prepared under acid (monoclinic form) and basic conditions (tetragonal form), the zirconia phase does not seem to play a direct role on the catalytic activity. Taking into account the structural analysis detailed above, we can conclude that the most active species for this reaction are the W(VI) species in tetrahedral coordination, present in both samples annealed at 500°C. For the as-synthesized samples, which also contain W(VI) tetrahedral species, the presence of hydroxyl groups and other adsorbed species (carbonates) at the surface is detrimental to aldoxime dehydration. Furthermore, both the microcrystalline WO_3 nanoparticles on monoclinic ZrO_2 and the interconnecting polyoxotungstate clusters on tetragonal ZrO_2 detected at 800°C, are less active than the tetrahedral species.

10WZA500 and 10WZU500 spent catalyst were calcined at 500°C and its structural and catalytic activities were further studied. Figure S18 and S19 show the XRD patterns and Raman spectra of these catalysts. For 10WZA500 no structural differences can be observe compared to the fresh one while for 10WZU500 small amounts of most thermodynamically stable monoclinic phase is observed in Raman spectra which is not visible by XRD. The catalytic activity of these materials are almost identical than the fresh catalysts (Table 3 and Table 4)

The reference samples (Table S6) show lower activity than our microwave-synthesized materials. Comparisons are arduous with the Sn-W oxide that shows a totally different structure, but in the case of W/ZrO_2 samples prepared by coprecipitation and impregnation methods, the materials exhibit similar tetragonal phase and S_{BET} area as the microwave-derived WZU materials. However, reference samples show larger zirconia crystallite sizes. These results suggest that the increased size of ZrO_2 crystallites is detrimental to the W dispersion and therefore for the catalytic activity and selectivity.

2.2.2 Hydration of alkynes

The catalytic activity of all materials was also tested for the hydration of alkynes, and more specifically for hydration of phenylacetylene (Scheme 3).

In this reaction, only W-doped zirconias annealed at 800°C showed good results (Table 5). The best activity (98%) and selectivity (89%) were obtained with the 10WZU-800 sample (100% *t*-ZrO_2). The sample 10WZA800 (87% *m*-ZrO_2) exhibits lower activity, which indicates that the tetragonal phase is more favorable for the catalysis of phenyl acetylene hydration.

10WZU800 spent catalyst calcined at 800°C presents a small amount of monoclinic zirconia not observed in the fresh catalyst(Figure S18 and S19), moreover some WO_X evolves to crystalline WO_3. The catalytic activity suffers a slight decrease probably caused by these structural changes.

The reference materials also show activities and selectivities as good as for the 10WZU-800 sample (Table S7). SnW 2:1 annealed at 800°C presents lower selectivity toward the desired product (84%), even with 3 times larger amount of W than the microwave-derived materials. The good results of the 10WZDep800 and 10WZDis800 samples point out that the tetragonal phase has a clear beneficial role on this catalysis.

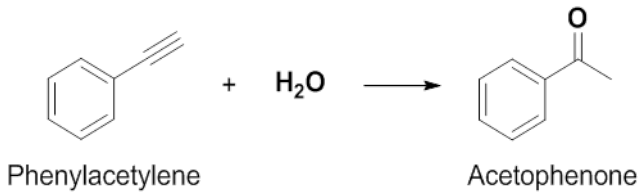

Scheme 3: Hydration of phenylacetylene.

Table 5. Conversion, yield and selectivity towards acetophenone in hydration of phenylacetylene of X-WZA-Y and X-WZU-Y samples. Reaction conditions: Catalyst 50 mg, 0.50 mmol Phenylacetylene, 2.5 mmol water, dodecane as standard, 1.5 mL cyclooctane, 95°C, 5 hours.

Catalyst	X Phenylacetylene (%)	Y Acetophenone (%)	Sel.Acetophenone (%)
5WZA800	16.9	11.7	68.9
10WZA500	6.2	0.2	2.5
10WZA800	65.5	55.7	85.0
5WZU800	43.6	37.4	85.8
10WZU500	10.4	0.7	7.1
10WZU800	**97.7**	**87.4**	**89.4**
10WZU800used	99.3	83.0	83.6

Pure zirconias and W(VI) species in tetrahedral coordination are not active in the alkyne hydration, probably due to the highly acidic character required for the catalyst to activate this reaction. Even at 800°C, where 10WZA800 and 10WZU800 samples behaves like a strong acid[38 41], their activities are different. The material with the tetragonal phase (10WZU800) is the most active. This behavior is in good agreement with previous works reporting that the activity of materials prepared by impregnating tungsten salts over crystalline monoclinic zirconia is much lower than those impregnated in the hydrous support,[12 45 49] which develops tetragonal phase upon annealing. In order to confirm this hypothesis, pure monoclinic and tetragonal ZrO_2 were synthesized,[46] wet impregnated with 10 wt. % of a W salt and annealed at 800°C (10WZM800 and 10WZT800 respectively). Figure 8 shows that the most active material in this reaction is 10WZU800, followed by 10WZT800, 10WZA800 and 10WZM800. By plotting the yield of acetophenone *versus* the tetragonal phase percentage (Figure 9), one can observe that the catalytic activity increases with increasing content of tetragonal ZrO_2, thus confirming the primary role of this polymorph.

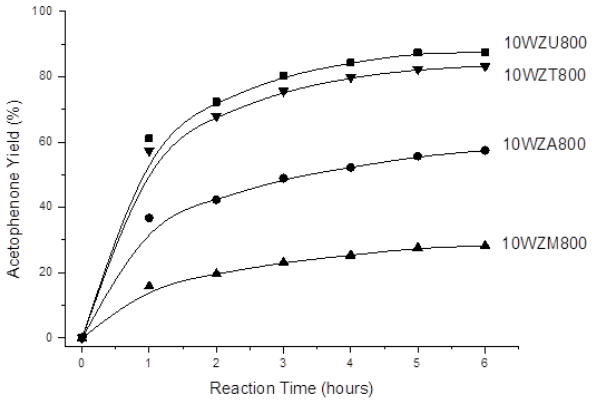

Figure 8. Kinetics plots for the hydration of phenylacetylene. Reaction Conditions: 0.5 mmol of phenylacetylene, 2.5 mmol of water, 1.5 Ml of cyclooctane, dodecane as standard and 95°C.

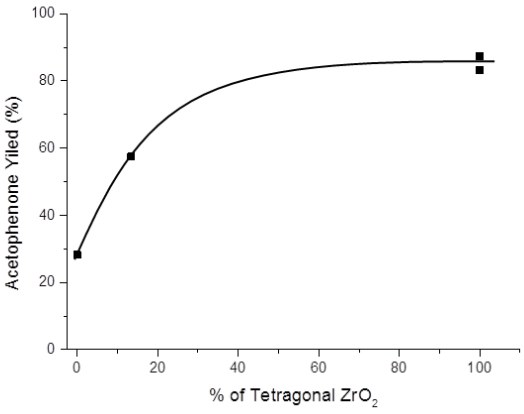

Figure 9. Acetophenone yield (reaction time 5 hours) as a function of tetragonal ZrO_2 content.

Several authors have studied the influence of the zirconia polymorphs in supported Cu,[63–65] Au,[66] Ag,[67] Rh,[68] and Mo[51]

catalysts. According to these studies, the species isolated on the tetragonal polymorph tend to exhibit a more cationic character than those isolated on the monoclinic phase with a higher metallic character. The reason for this trend lies in the presence of anion vacancies in the metastable tetragonal polymorph originating from the introduction of trivalent or divalent ions.[69] As a consequence, the more ionic character of the tetragonal polymorph induces higher Lewis and Brønsted acidity[63] (see Figure S8 and Table S3) than in the more covalent monoclinic structure. Thus the more acid species stabilized over the tetragonal zirconia could explain the higher activity in the hydration of alkynes.

The better activity of 10WZU800 sample than 10WZT800 reference (both pure *t*-ZrO_2) reveals differences in the active W-based clusters. According to the previous work of Kiely and co-workers,[49] the catalytic active species in the alkane isomerization reaction are 0.8-1 nm WO_x clusters incorporating some Zr(IV) cations. In our experiments, the active species for alkyne hydration are interconnected polyoxotungstate clusters on *t*-ZrO_2. We suggest that the microwave-assisted technique allows the partial incorporation of zirconium cations within these small polyoxotungstate clusters. Indeed, the high heating efficiency of microwave heating levers the different reactivities of zirconium and tungsten soluble precursors. Consequently, the formation of mixed Zr-W oxide frameworks is more likely than in conventional heating with slower heating ramps and nucleation rates. As a consequence, both the predominance of the tetragonal crystalline zirconia phase and the presence of Zr-W oxoclusters would be responsible for the improved catalytic properties of the microwave-derived 10WZU800 catalyst in the hydration of alkynes.

3. Conclusions

To conclude, different W-ZrO_2 materials were synthesized by a microwave-assisted aqueous route for the first time. The variation of different synthetic parameters (pH of the reaction medium, the W- doping level, further thermal treatment…) allows obtaining selectively zirconia in its tetragonal or monoclinic polymorphs. This results in a change in the nature of the tungsten species dispersed on the ZrO_2 nanoparticles.

The performances of these materials as catalysts were tested for the aldoxime dehydration and alkyne hydration reactions and compared with reference materials. For the aldoxime dehydration, the most active materials were those having W(VI) species in tetrahedral coordination, mainly found in samples annealed at 500°C, and the zirconia polymorph did not show any significant impact on the activity.

On the contrary, in the alkyne hydration, the active species seem to be the interconnected polyoxotungstate clusters and microcrystalline WO_3 supported on the tetragonal polymorph, which are more acid than the W species supported on monoclinic zirconia. This strong effect may arise from the more ionic character of the tetragonal phase compared to the monoclinic one, which exacerbates the acidic character of supported W species. Furthermore, the microwave-assisted methodology seems to facilitate the incorporate of Zr^{4+} ions in the WO_x clusters located on the tetragonal polymorph, thus resulting in highly active mixed cationic active sites.

Acknowledgements

F.G. is grateful to Ministerio de Educación, Cultura y Deporte for his PhD grant (AP2010-2748), B.J.L. and F.G. thank the Spanish Government (MAT2011-27008 project) and University Jaume I (UJI, P1 1B2014-21). F.G. and A.C. thank financial support from Spanish Government-MINECO through "Severo Ochoa" (SEV 2012-0267). D.P., C.S. and K.V. would like to strongly acknowledge the Foundation du Collège de France for support and thank the French Commissariat à l'Energie Atomique et aux Energies Alternatives for financial support. SCIC from Universitat Jaume I and Servicio de Microscopía Electrónica at Universitat Politècnica de València are also acknowledged for instrumental facilities.

Notes and references

1 S. Shukla and S. Seal, *Int. Mater. Rev.*, 2005, **50**, 1–20.
2 G. Postole, B. Chowdhury, B. Karmakar, K. Pinki, J. Banerji and A. Auroux, *J. Catal.*, 2010, **269**, 110–121.
3 J. García, P. Quintana, D. H. Aguilar, T. López and R. Gómez, *J. Sol-Gel Sci. Technol.*, 2006, **37**, 185–188.
4 S. Liu, J. Ma, L. Guan, J. Li, W. Wei and Y. Sun, *Microporous Mesoporous Mater.*, 2009, **117**, 466–471.
5 P. Thangadurai, A. Chandra, Bose and S. Ramasamy, 2005, **0**, 3963–3968.
6 a. Ghosh, a. K. Suri, M. Pandey, S. Thomas, T. R. Rama Mohan and B. T. Rao, *Mater. Lett.*, 2006, **60**, 1170–1173.
7 B. M. Reddy and M. K. Patil, *Chem. Rev.*, 2009, **109**, 2185–208.
8 K. Chen, S. Xie, E. Iglesia and A. T. Bell, *J. Catal.*, 2000, **189**, 421–430.
9 M. Scheithauer, R. K. Grasselli and H. Knözinger, *Langmuir*, 1998, 3019–3029.
10 G. Larsen, E. Lotero, R. D. Parra, L. M. Petkovic, H. S. Silva and S. Raghavan, *Appl. Catal. A Gen.*, 1995, **130**, 213–226.
11 M. Hino and K. Arata, *J. Chem. Soc., Chem. Commun*, 1988, 1259.
12 K. Arata and M. Hino, *Proc. 9th Int. Congr. Catal. Calgary, Canada, 1988; Philips, M. J., Ternan, M., Eds.; Chem. Inst. Canada, Ottawa, Canada*, 1988, 1727.
13 Z. Hasan, J. Jeon and S. H. Jhung, *J. Hazard. Mater.*, 2012, **205-206**, 216–21.
14 S. Sarish, B. M. Devassy, W. Böhringer, J. Fletcher and S. B. Halligudi, *J. Mol. Catal. A Chem.*, 2005, **240**, 123–131.
15 D. G. Barton, S. L. Soled, G. D. Meitzner, G. A. Fuentes and E. Iglesia, *J. Catal.*, 1999, **181**, 57–72.
16 D. Wang, C. M. Osmundsen, E. Taarning and J. a. Dumesic, *ChemCatChem*, 2013, **5**, 2044–2050.
17 C. D. Baertsch, K. K. T, Y. Chua and E. Iglesia, *J. Catal.*, 2002, **205**, 44–57.
18 K. Friedrich and K. Wallenfels, *The Chemistry of the Cyano Group*, New York, Wiley-Inte., 1970.
19 A. Fatiadi, *Preparation and synthetic applications of cyano compounds*, New York, Wiley., 1983.
20 P. Yan, G. K. Batamack, S. Prakash and G. A. Olah, *Catal. Letters*, 2005, **101**, 141–143.
21 S. H. Yang and S. Chang, *Org. Lett.*, 2001, **3**, 4209–4211.
22 K. Ishihara, Y. Furuya and H. Yamamoto, *Angew. Chemie Int. Ed.*, 2002, **41**, 2983–2986.
23 D. Li, F. Shi, S. Guo and Y. Deng, *Tetrahedron Lett.*, 2005, **46**, 671–674.
24 R. Rezaei and M. Karami, *Chinese Chem. Lett.*, 2011, **22**, 815–818.
25 B. Thomas, S. Prathapan and S. Sugunan, *Microporous Mesoporous Mater.*, 2005, **79**, 21–27.

26 E. Choi, C. Lee, Y. Na and S. Chang, *Org. Lett.*, 2002, **4**, 2369–2371.
27 K. Yamaguchi, H. Fujiwara, Y. Ogasawara, M. Kotani and N. Mizuno, *Angew. Chem. Int. Ed. Engl.*, 2007, **46**, 3922–5.
28 M. Berthelot, *Acad. Sci. C. R.*, 1860, 805–808.
29 M. Kutscheroof, *Ber. Dtsch. Chem. Ges*, 1884, **17**, 13.
30 G. F. Hennion, D. B. Killian, T. H. Vaughn and J. A. Nieuwland, *J. Am. Chem. Soc.*, 1934, **56**, 1786.
31 N. Marion, R. S. Ramo and S. P. Nolan, *J. Am. Chem. Soc.*, 2009, **131**, 448–449.
32 T. Suzuki, M. Tokunaga and Y. Wakatsuki, *Org. Lett.*, 2001, **3**, 735–737.
33 J. R. Cabrero-Antonino, A. Leyva-Pérez and A. Corma, *Chem. Eur. J.*, 2012, **18**, 11107–14.
34 S. Iimura, K. Manabe and S. Kobayashi, *Org. Biomol. Chem.*, 2003, **1**, 2416–2418.
35 J. Huang, F. Zhu, W. He, F. Zhang, W. Wang and H. Li, *J. Am. Chem. Soc.*, 2010, **132**, 1492–1493.
36 K. T. V. Rao, P. S. S. Prasad and N. Lingaiah, *Green Chem.*, 2012, **14**, 1507–1514.
37 X. Jin, T. Oishi, K. Yamaguchi and N. Mizuno, *Chem. Eur. J.*, 2011, **17**, 1261–7.
38 A. Corma, *Chem. Rev.*, 1995.
39 F. Figueras, J. Palomeque, S. Loridant, C. Fèche, N. Essayem and G. Gelbard, *J. Catal.*, 2004, **226**, 25–31.
40 S. Loridant, C. Feche, N. Essayem and F. Figueras, *J. Phys. Chem. B*, 2005, **109**, 5631–5637.
41 M. A. Cortés-Jácome, C. Angeles-Chavez, E. López-Salinas, J. Navarrete, P. Toribio and J. A. Toledo, *Appl. Catal. A Gen.*, 2007, **318**, 178–189.
42 J. G. Santiesteban, J. C. Vartuli, S. Han, R. D. Bastian and C. D. Chang, *J. Catal.*, 1997, **441**, 431–441.
43 M. A. Cortés-Jácome, J. A. Toledo, C. Angeles-Chavez, M. Aguilar and J. A. Wang, *J. Phys. Chem. B*, 2005, **109**, 22730–9.
44 R. A. Boyse and E. I. Ko, *J. Catal.*, 1997, **171**, 191–207.
45 V. Lebarbier, G. Clet and M. Houalla, *J. Phys. Chem. B*, 2006, **110**, 13905–11.
46 W. Li, H. Huang, H. Li, W. Zhang and H. Liu, *Langmuir*, 2008, **24**, 8358–66.
47 M. a. Cortés-Jácome, C. Angeles-Chavez, X. Bokhimi and J. a. Toledo-Antonio, *J. Solid State Chem.*, 2006, **179**, 2663–2673.
48 N. Soultanidis, W. Zhou, A. C. Psarras, A. J. Gonzalez, E. F. Iliopoulou, C. J. Kiely, I. E. Wachs and M. S. Wong, *J. Am. Chem. Soc.*, 2010, **132**, 13462–71.
49 W. Zhou, E. I. Ross-Medgaarden, W. V Knowles, M. S. Wong, I. E. Wachs and C. J. Kiely, *Nat. Chem.*, 2009, **1**, 722–728.
50 Y. Ogasawara, S. Uchida, K. Yamaguchi and N. Mizuno, *Chem. Eur. J.*, 2009, **15**, 4343–9.
51 W. Li, H. Huang, H. Li, W. Zhang and H. Liu, *Langmuir*, 2008, **24**, 8358–8366.
52 J.-L. Tosan, B. Durand, M. Roubin, F. Chassagneux, L. Mosoni, F. Bertin and B. Moraweck, *J. Non. Cryst. Solids*, 1993, **160**, 167–176.
53 J.-L. Tosan, B. Durand, M. Roubin, F. Chassagneux and F. Bertin, *J. Non. Cryst. Solids*, 1994, **168**, 23–32.
54 P. D. Southon, J. R. Bartlett, J. L. Woolfrey and B. Ben-Nissan, *Chem. Mater.*, 2002, **14**, 4313–4319.
55 M. Ambrosi, E. Fratini, P. Canton, S. Dankesreiter and P. Baglioni, *J. Mater. Chem.*, 2012, **22**, 23497.
56 L. M. Thot, J. S. Lin and L. K. Felker, *J. Phys Chem*, 1991, **95**, 3106–3108.
57 A. Clearfield and P. A. Vaughan, *Acta Crystallogr.*, 1956, **9**, 555–558.
58 K. T. Jung and A. T. Bell, *J. Mol. Catal. A Chem.*, 2000, **163**, 27–42.
59 A. Clearfield, G. P. D. Serrette and A. H. Khazi-Syed, *Catal. Today*, 1994, **20**, 295–312.
60 J. Livage and C. Mazieres, *J. Am. Ceram. Soc.*, 1968, **51**, 349–353.
61 R. P. Denkewicz, K. S. TenHuisen and J. H. Adair, *J. Mater. Res.*, 1990, **5**, 2698–2705.
62 J.-P. Jolivet, *De la solution à l'oxyde*, EP Sciences-CNRS Editions, Paris, 2015.
63 K. Samson, M. Sliwa, R. P. Socha, K. Góra-Marek, D. Mucha, D. Rutkowska-Zbik, J.-F. Paul, M. Ruggiero-Mikolajczyk, R. Grabowski and J. Sloczynski, *ACS Catal.*, 2014, **4**, 3730–3741.
64 M. D. Rhodes and A. T. Bell, *J. Catal.*, 2005, **233**, 198–209.
65 M. D. Rhodes, K. A. Pokrovski and A. T. Bell, *J. Catal.*, 2005, **233**, 210–220.
66 J. Li, J. Chen, W. Song, J. Liu and W. Shen, *Appl. Catal. A Gen.*, 2008, **334**, 321–329.
67 R. Grabowski, J. Sloczynski, M. Sliwa, D. Mucha and R. P. Socha, *ACS Catal.*, 2011, **1**, 266–278.
68 M. C. Campa, G. Ferraris, D. Gazzoli, I. Pettiti and D. Pietrogiacomi, *Appl. Catal. B Environ.*, 2013, **142-143**, 423–431.
69 B. Julián-López, V. De La Luz, F. Gonell, E. Cordoncillo, M. López-Haro, J. J. Calvino and P. Escribano, *J. Alloys Compd.*, 2012, **519**, 29–36.